Am J Transl Res 2025;17(11):8724-8741
www.ajtr.org /ISSN:1943-8141/AJTR0168563

Original Article

MEGF8-driven metabolic reprogramming and immune evasion define a high-risk subtype of endometriosis-associated ovarian cancer

Bo Zheng[1*], Yu Xia[1*], Yuxuan Feng[2*], Yanqiu Zhang[3*], Haoyue Hu[4], Bing Jiang[4], Meng Liu[5], Nianchao Zhou[4], Tiantian Wu[1], Guannan Feng[5], Chao Huang[1], Qingxia Meng[1], Xiaoyan Huang[2]

[1]State Key Laboratory of Reproductive Medicine and Offspring Health, Center for Reproduction and Genetics, The Affiliated Suzhou Hospital of Nanjing Medical University, Suzhou Municipal Hospital, Gusu School, Nanjing Medical University, Suzhou 215002, Jiangsu, China; [2]State Key Laboratory of Reproductive Medicine and Offspring Health, Department of Histology and Embryology, School of Basic Medical Sciences, Nanjing Medical University, Nanjing 211166, Jiangsu, China; [3]Institute of Clinical Pharmacology, Anhui Medical University, Key Laboratory of Anti-inflammatory and Immune Medicine, Ministry of Education, Anhui Collaborative Innovation Center of Anti-inflammatory and Immune Medicine, Hefei 230032, Anhui, China; [4]Human Reproductive and Genetic Center, Affiliated Hospital of Jiangnan University, Wuxi 214062, Jiangsu, China; [5]Department of Gynecology, The Affiliated Suzhou Hospital of Nanjing Medical University, Suzhou Municipal Hospital, Gusu School, Nanjing Medical University, Suzhou 215002, Jiangsu, China. [*]Equal contributors.

Received September 4, 2025; Accepted October 23, 2025; Epub November 15, 2025; Published November 30, 2025

Abstract: Objective: Endometriosis increases ovarian cancer (OC) risk through genetic mutations, chronic inflammation, and hormonal dysregulation, yet the underlying molecular pathways remain underexplored. This study aims to identify endometriosis-associated prognostic biomarkers in OC. Methods: Transcriptomic and clinical data from TCGA-OC and GSE53963 were integrated for comprehensive analysis. Prognostic models were constructed using LASSO and Cox regression. Tumor microenvironment (TME) characteristics, immune checkpoints, and drug sensitivity were evaluated with ESTIMATE, CIBERSORT, TIDE, and drug sensitivity profiling. Single-cell RNA sequencing (scRNA-seq, GSE184880) was employed to explore immune and gene expression patterns. MEGF8 function was validated through *in vitro* assays. Results: Consensus clustering identified three OC molecular subtypes (A, B, and C), with subtype B showing significantly better overall survival (P = 0.001). Subtype A exhibited a "dual malignant phenotype", characterized by enhanced cell adhesion, epithelial-mesenchymal transition (EMT), TGF-β activation, and an immunosuppressive TME. An 8-gene prognostic model, including MEGF8, effectively stratified patients into high- and low-risk groups, with high-risk patients showing poorer survival, immune evasion, and elevated stromal scores. Drug sensitivity analysis indicated that the low-risk group was more responsive to PI3K/AKT/mTOR and VEGFR inhibitors. MEGF8 was identified as a key regulator in cancer stem cells, promoting tumor progression through metabolic reprogramming and extracellular matrix remodeling. Functionally, MEGF8 knockdown suppressed OC cell proliferation and migration. Conclusion: This study delineated the molecular-immune landscape of OC, established an 8-gene prognostic model, and identified MEGF8 as a potential therapeutic target. The model predicts responses to immunotherapy and targeted therapies, supporting personalized OC management.

Keywords: Endometriosis, ovarian cancer, MEGF8, biological behavior, prognostic model, single-cell RNA sequencing

Introduction

Ovarian cancer (OC) remains a leading cause of death among gynecologic malignancies, accounting for over 200,000 deaths annually worldwide. Its clinical management is challenged by two major obstacles: first, the disease often presents with insidious symptoms, resulting in approximately 70% of patients being diagnosed at advanced stages (FIGO stage III-IV), where the five-year survival rate drops below 30%; second, the marked intratumoral heterogeneity and development of chemoresistance significantly increase the risk of

https://doi.org/10.62347/AOPY5249

therapeutic failure [1-5]. Although cytoreductive surgery combined with platinum-based chemotherapy can offer temporary remission, approximately 80% of patients ultimately experience relapse and treatment resistance, leading to poor overall survival (OS) [6]. Recent studies have suggested that the molecular heterogeneity of OC arises not only from histologic subtypes (e.g., high-grade serous carcinoma, endometrioid carcinoma) but also is tightly linked to its cell-of-origin and microenvironmental context. Endometriosis - a well-established risk factor - can increase the incidence of OC by 3- to 5-fold compared to the general population and is often associated with distinct features such as metabolic reprogramming and immune evasion [7, 8]. However, a comprehensive molecular classification system specifically for endometriosis-associated OC remains lacking. The regulatory gene networks and tumor-microenvironment interactions driving its malignant progression are poorly understood, representing a major barrier to the development of effective targeted therapy. Therefore, it is of clinical importance to leverage integrative multi-omics approaches to delineate the molecular landscape of this OC subtype, identify actionable targets, and establish prognostic models to guide precision medicine.

Endometriosis, a prevalent chronic inflammatory disease affecting women of reproductive age - with a global prevalence of approximately 10% and up to 40% among infertile populations - not only causes pelvic pain and infertility but is also increasingly recognized as a precursor condition for OC [9-11]. Pathologic studies have demonstrated that ectopic endometrial tissues undergo a vicious cycle of “repeated hemorrhage-inflammation-fibrosis”, which fosters local oxidative stress and aberrant cellular proliferation, ultimately driving malignant transformation [12]. Recent genomic and epidemiologic studies further support this link, revealing that women with endometriosis face a 3- to 8-fold higher risk of developing OC compared to the general population [13]. These two conditions also share critical molecular vulnerabilities, including frequent mutations in KRAS and ARID1A, as well as epigenetic dysregulation such as aberrant methylation within the HOX gene clusters [13-15]. Notably, endometriosis-associated OC represents a distinct molecular subtype of OC: approximately 60% of ovarian clear cell carcinoma and endometrioid carcinoma cases coexist with endometriosis and are frequently characterized by activation of the Phosphoinositide 3-Kinase (PI3K)/Protein Kinase B (AKT)/Mammalian Target of Rapamycin (mTOR) signaling axis and an immunosuppressive tumor microenvironment [16, 17]. However, the regulatory gene networks, dynamic tumor microenvironment (TME) remodeling, and clinically relevant prognostic biomarkers underlying endometriosis-associated OC remain poorly elucidated. This lack of systematic characterization poses a major barrier to the development of effective precision medicine strategies.

In response to the above mechanistic links and clinical challenges, this study integrates multi-omics datasets - including bulk transcriptomic profiles and single-cell RNA sequencing (scRNA-seq) - with functional validation platforms to construct a comprehensive regulatory framework of endometriosis-associated ovarian cancer (EAOC), spanning molecular subtyping, microenvironmental remodeling, and therapeutic responsiveness. We systematically identified a set of endometriosis-related genes (ERGs) shared between endometriosis and OC, and established an interpretable prognostic model using LASSO-Cox regression. Incorporating TME features - such as immune checkpoint expression and T cell exhaustion scores - we further evaluated the potential of ERGs as predictive biomarkers for immunotherapeutic response and as stratification tools for PI3K/AKT-targeted therapies. Focusing on the core regulator MEGF8, we combined single-cell transcriptomic analysis with *in vitro* models to reveal its role in sustaining cancer stem cell plasticity through a “metabolism-extracellular matrix (ECM) remodeling axis”, characterized by enhanced oxidative phosphorylation and extracellular matrix reorganization. Collectively, our findings provide novel insight into the molecular underpinnings of OC and lay a translational foundation for precision oncology strategies aimed at overcoming therapeutic resistance and improving patient outcomes.

Materials and methods

Identification of endometriosis-related genes (ERGs)

The GSE7305 dataset, comprising ten normal and ten endometriotic human endometrial tis-

sue samples, was analyzed for differential gene expression using the limma package. Statistically significant genes were identified based on thresholds of $|\log_2$ fold change (FC)| > 1 and adjusted *p* value < 0.05.

Collection of OC data

Gene expression data and matched clinical information data were acquired from The Cancer Genome Atlas (TCGA) and Gene Expression Omnibus (GEO) (GSE53963) databases. Patients with OS times and status were included in the study. ERGs were acquired from a previous study. Copy number variation (CNV) data and somatic mutations were downloaded from TCGA-OV.

Consensus clustering to identify ERG clusters

Based on the expression levels of ERGs, a consensus unsupervised clustering analysis was performed using the R package "ConsensusCluster-Plus" to categorize patients into different endometriosis related clusters [18]. The number of classifications depended on the increase in intra-group correlations and the decrease in inter-group correlations.

Functional enrichment and immune cell infiltration analysis

R package "GSVA" was utilized for gene set variation analysis (GSVA), performed with "c2.cp.kegg.symbols" and "c5.go.symbols", and heatmaps of GSVA were plotted using R software [19]. Single-sample gene set enrichment analysis (ssGSEA) was performed to explore immune infiltration in different endometriosis clusters.

Identification of endometriosis gene clusters in OC

Differentially expressed genes (DEGs) between endometriosis clusters were identified using the R package "Limma". The significance criterion was set at $|\log_2$ FC| > 0.5 and adjusted *p*-value < 0.05. Univariate Cox regression analyses were performed to identify DEGs associated with OS in endometriosis clusters. According to the expression levels of OS-related DEGs, we performed consensus unsupervised clustering analysis to classify OC patients into different endometriosis gene clusters using R package "ConsensusClusterPlus".

Construction of the prognostic risk model

OC patients in the TCGA and GSE53963 databases were randomly assigned to train and test groups (1:1). The R package "glmnet" was used to perform the least absolute shrinkage and selection operator (LASSO) to screen out the characterized genes for constructing the prognostic risk model. The prognostic risk score was calculated based on gene expression and correlation coefficient (risk score = expression * coefficient for each gene), and patients were categorized into high-risk and low-risk groups based on the median risk score. R packages "survival" and "survminer" were used to compare the survival probabilities of the two groups by Kaplan-Meier analysis. R package "timeROC" was employed to perform 1-, 3- and 5- year receiver operating characteristic (ROC) analysis and calculate the value of the area under the curve (AUC).

Assessment of TME scores, immune correlation analysis, and chemotherapy effects

Mutation information for OC was obtained from the TCGA database and analyzed using the R package "maftools" to demonstrate the mutational landscape of the high and low risk groups. The ESTIMATE algorithm was used to calculate the stromal Score, immune Score, and estimate Score using the "estimate" R package [20]. CIBERSORT algorithm was used to quantify the immune infiltration of different groups [21]. Then, we assessed the correlation of immune cell infiltration with risk scores and signature genes in the prognostic risk model using the Spearman rank correlation coefficient. In addition, the Wilcoxon test assessed differential expression of immune checkpoint genes between high- and low-risk groups. Immunotherapy response in OC patients was estimated by the Tumor Immune Dysfunction and Exclusion (TIDE) algorithm (http://tide.dfci.harvard.edu). Using the pRRophetic R package in R (version 4.1.0), the IC50 for the effect of molecular therapy and chemotherapy was calculated and compared between the high- and low-risk groups.

Single-cell sequencing analysis

The scRNA-seq dataset GSE184880 was downloaded from the GEO database for analysis. Employing the Seurat R package [22], we

performed an integrated computational workflow for single-cell transcriptomic profiling. Cells with a gene count (nFeature RNA) ≤ 300 or ≥ 5000 and a mitochondrial gene proportion of less than 10% were screened, while cells identified as low quality were excluded from the dataset. After scaling the gene expression levels, we normalized the data using the "LogNormalize" function and performed principal component analysis (PCA) [23]. The harmony package [24] was employed to mitigate batch effects across different samples. Cell clustering and dimensionality reduction were performed with the "FindClusters" and "RunUMAP" functions. The "SingleR" package and CellMarker were used as a reference for cell annotation.

Cell culture and treatments

Human OC cell lines (OVCAR3, A2780) were obtained from the Chinese Academy of Cell Collection (Shanghai, China), and cultured in a humidified condition at 37°C with 5% CO_2. OVCAR3 cells was cultivated in RPMI-1640 (Gibco, USA) with fetal bovine serum (FBS) (ExCell Bio, New Zealand) and 1% penicillin/streptomycin (PS) (NCM Biotech, China). Specifically, 10% FBS was needed to A2780, and 20% to OVCAR3. Dulbecco's modified Eagle medium (Gibco, USA) with 10% FBS and 1% PS were used to culture A2780 cells. When the cell fusion degree reached 60-70%, small interfering RNAs (siRNAs) (GenePharma, Suzhou, China) targeting RNA interference and transfection the small interfering RNAs of MEGF8 obtained from Suzhou GenePharma Co., Ltd. (Suzhou, China). siRNA was transfected into A2780 and OVCAR3 cells by using Lipofectamine 2000 (Invitrogen, USA). Knockdown efficiency was evaluated by quantitative real-time polymerase chain reaction (qRT-PCR).

The siRNA target sequences were as follows: si-MEGF8-1#: 5'-CGCUGUAAGUGGUGUACCA-3', si-MEGF8-2#: 5'-GUGCGUAACUGCCAGAAUAA-3', si-NC: 5'-UUCUCCGA ACGUGUCACGU-3'.

RNA extraction and qRT-PCR

TRIzol reagent (Vazyme, Nanjing, China) was used to extract RNA from transfected A2780 and OVCAR3 cells. Next, a reverse transcription kit (Vazyme, Nanjing, China) was used to reverse transcribe the RNA into cDNA following the manufacturer's instructions. Taq Pro Universal SYBR qPCR Master Mix (Vazyme, Nanjing, China) was used for qRT-PCR detection and quantification of gene expression using a qRT-PCR system (Applied Biosystems, Inc, Foster City, CA, USA). 18S rRNA was used as the internal reference. The primers used were as follows: 18sRNA-F: 5'-AAACG GCT ACC ACA TCC AAG-3', 18sRNA-R: 5'-CCTCC AAT GGA TCC TCGTT A-3', MEGF8-F: 5'-GACAGTGCTGCC-TGGAAGAT-3', MEGF8-R: 5'-CGCGAAGGGAAG-ATGCAAAG-3'.

Cell proliferation assays

A 96-well plate (2000 cells/well) was inoculated with the cells for the Cell Counting Kit-8 (CCK-8) assay. Cell viability was measured every 24 h using a CCK-8 kit (Beyotime) on a microplate reader (Bio-Rad Model 680, USA) at 450 nm, as previously described [25-27].

800-1000 cells were added into six-well plates for 2 weeks to evaluate cloning formation capabilities. The clones were fixed with methanol, stained with 0.1% crystal violet (Beyotime) and counted for analysis.

Cell migration assays

In the transwell assay, 4.5×10^4 cells in 300 μl serum-free medium were seeded into the upper chamber with 8 μm pore size (Corning, USA), whereas 700 μl complete medium was added into the lower chamber. After 48 h, the cells outside the chamber were fixed, stained and imaged for counting.

Statistical analyses

Statistical analyses were performed using R (version 4.1.0) and GraphPad Prism 8.0. Data are expressed as mean ± SD. Statistical comparisons between groups were made using Student's t-test or one-way ANOVA. The survival analysis was conducted using the Kaplan-Meier method, and log-rank tests were employed to identify the significance of differences. $P < 0.05$ was considered significant.

Results

Distinct molecular and immune landscapes in endometriosis-derived OC predict clinical outcomes

A total of 1,483 DEGs were identified in endometriotic ovarian tissues compared to normal ovarian tissues, including 814 upregulated and

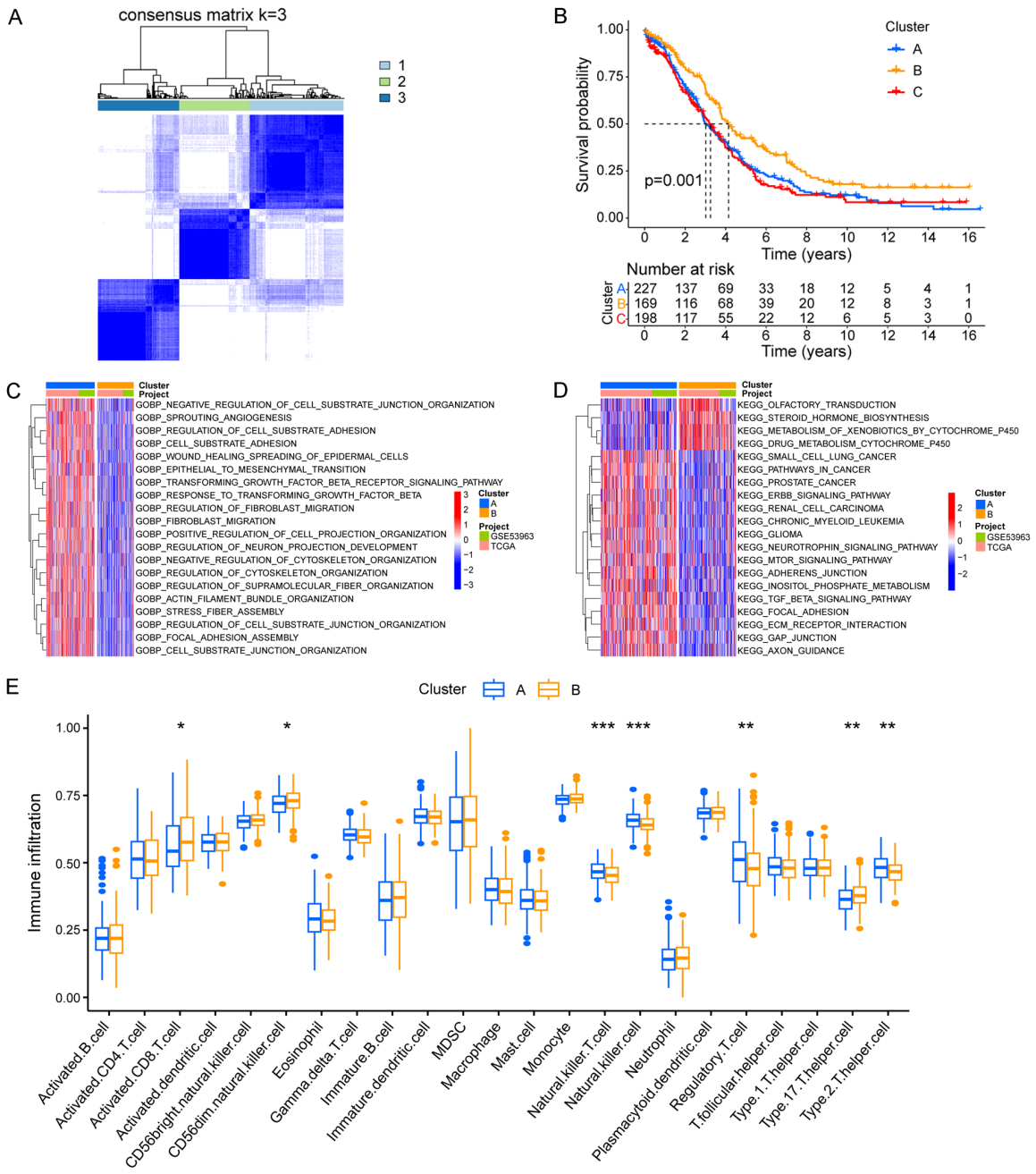

Figure 1. Endometriosis clusters with distinct prognostic and immune infiltration characteristics. A. Three endometriosis clusters were identified using consensus clustering analyses. B. Kaplan-Meier analysis indicated that the prognosis of cluster B was significantly better than that of cluster A. C. Gene Ontology (GO)-related gene set variation analysis (GSVA) showing the activation status of biological behaviors in endometriosis cluster A and B. D. Kyoto Encyclopedia of Genes and Genomes (KEGG)-related GSVA showing the activation status of biological behaviors in endometriosis cluster A and B. E. The abundance of each immune cell infiltration in endometriosis cluster A and B. ***P < 0.001; ns, P > 0.05.

669 downregulated DEGs. To investigate the expression features and potential biological characteristics of ERGs in OC, a consensus clustering algorithm was used to classify OC patients in the TCGA cohort and the GSE53963 cohort. Based on the expression of ERGs, OC patients were classified into 3 clusters, endometriosis cluster A, B and C (**Figure 1A**). As the Kaplan-Meier survival curves crossed, endometriosis cluster B demonstrated a significant-

ly better prognosis compared with clusters A and C (P = 0.001) (**Figure 1B**).

Given the marked prognostic differences between clusters A and B, these two groups were selected for further investigation. GSVA revealed distinct biological characteristics between the two clusters. As shown in **Figure 1C**, cluster A was primarily enriched in biological processes related to cell adhesion, migration, and cytoskeletal regulation, including focal adhesion assembly, cell-substrate junction organization, epithelial-to-mesenchymal transition, and regulation of the TGF-β signaling pathway, suggesting a potential role in tumor invasion and metastasis. Notably, Kyoto Encyclopedia of Genes and Genomes (KEGG) pathway analysis indicated that cluster A was significantly associated with cancer-related pathways, such as small cell lung cancer, prostate cancer, the mTOR signaling pathway, and ECM-receptor interaction, as well as with metabolic reprogramming pathways, including cytochrome P450-mediated drug metabolism (**Figure 1D**). These contrasting enrichment profiles suggest that aberrant activation of cell adhesion and migration within the TME, in combination with metabolic adaptation and dysregulation of key oncogenic signaling pathways, may contribute to disease progression.

To further investigate the immune landscape, ssGSEA was performed to evaluate immune cell infiltration across endometriosis clusters A and B. Significant differences in immune infiltration were observed between the two groups (**Figure 1E**). Cluster A exhibited lower infiltration levels of activated CD8 T cells, CD56 dim natural killer cells, and type 17 T helper cells, but higher levels of natural killer T cells, natural killer cells, regulatory T cells, and type 2 T helper cells, indicating that distinct immune microenvironment profiles may underlie the biological divergence of these subtypes.

Gene signature-driven risk stratification reveals survival heterogeneity in endometriosis-linked OC

Subsequently, the prognostic significance of DEGs between endometriosis clusters A and B was evaluated using univariate Cox regression analysis, resulting in the identification of 229 OS-related DEGs (P < 0.05). Based on the expression profiles of these OS-related DEGs, a consensus clustering approach was employed, and OC patients were stratified into three gene clusters, designated gene clusters A, B, and C (**Figure 2A**). Kaplan-Meier survival analysis confirmed that patients in gene cluster B exhibited the most favorable prognosis compared to those in clusters A and C (P = 0.001; **Figure 2B**).

Eight prognostic signature genes (GPC3, C2orf88, AFAP1L2, MEGF8, PLXND1, HEYL, PHLDB2, and ANTXR1) were subsequently selected through LASSO regression followed by multivariate Cox analysis, and were used to construct a prognostic risk model (**Figure 2C-E**). Somatic mutation analysis revealed that 20 of 462 samples (4.33%) harbored mutations in at least one of the eight signature genes (**Figure 2F**). In addition, CNV analysis demonstrated that HEYL had the highest frequency of amplification, while AFAP1L2 and MEGF8 showed a widespread frequency of CNV loss (**Figure 2G**).

The associations among molecular clusters, gene clusters, and risk scores were further explored. Risk scores were found to be significantly lower in endometriosis cluster B compared to cluster A (**Figure 2H**). Among the three gene clusters, the risk score followed the order: cluster C > cluster A > cluster B (**Figure 2I**).

Patients were subsequently categorized into high- and low-risk groups based on the median risk score. Risk distribution plots revealed that patients in the high-risk group were associated with increased mortality and shorter OS. Heatmap analysis further demonstrated distinct expression patterns of the eight signature genes between the high- and low-risk groups across the overall cohort, as well as in the training and test subsets (**Figure 3A-C**). Kaplan-Meier analysis showed that patients in the high-risk group had significantly worse OS compared to those in the low-risk group, in both the training and test cohorts (**Figure 3D-F**).

The predictive performance of the risk model was evaluated using time-dependent ROC curves. In the overall cohort, the AUC for predicting 1-, 3-, and 5-year OS was 0.595, 0.636, and 0.643, respectively (**Figure 3G**). In the training cohort, the corresponding AUC values were 0.655, 0.664, and 0.686 (**Figure 3H**), and in the test cohort, the AUC values were 0.547, 0.604, and 0.605 (**Figure 3I**).

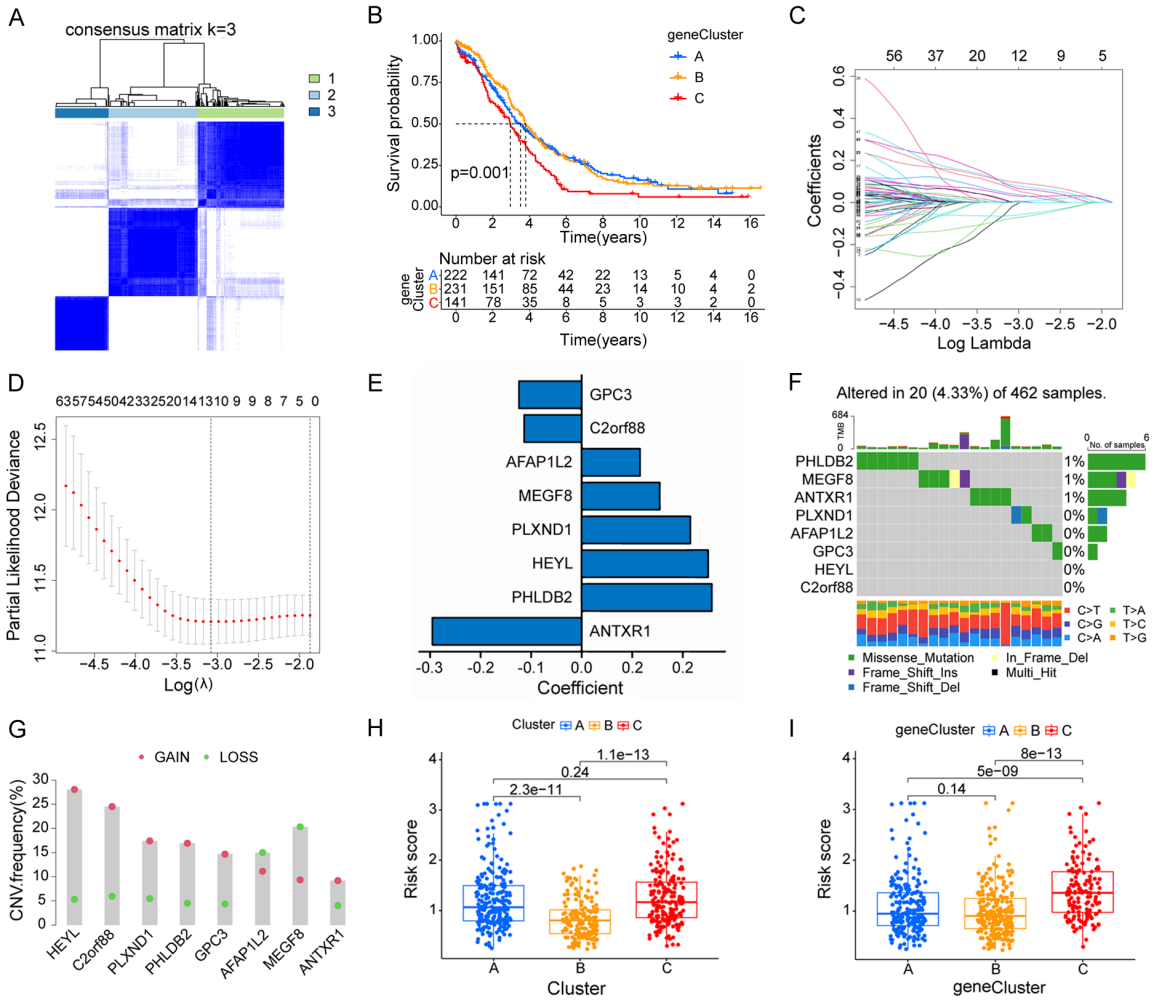

Figure 2. Gene clusters derived from differentially expressed genes (DEGs) and the establishment of an 8-gene prognostic signature model. A. Heatmap of the consensus matrix defining three gene clusters (k = 3). B. The three gene clusters' Kaplan-Meier overall survival (OS) curves (P = 0.001). C. Cross-validation of least absolute shrinkage and selection operator (LASSO regression parameter selection). D. Endometriosis-related genes (ERGs) regression using LASSO. E. The coefficients of the 8 signature genes. F. Mutation frequencies of 8 signature genes. G. Frequencies of copy number variation (CNV) increases and deletions and non-CNV among the 8 signature genes. H. Variations in risk scores among endometriosis clusters. I. Variations in risk scores among different gene clusters.

Integrative analysis of immune evasion and drug response in molecularly defined OC subtypes

Next, tumor mutation burden (TMB) was investigated within the context of the prognostic risk model. The mutation waterfall plot revealed that TP53 mutations were observed in 87% of patients in the high-risk group, compared to 82% in the low-risk group, indicating a higher mutation frequency among high-risk patients (**Figure 4A**). Components of the TME, including stromal and estimate scores, were significantly elevated in the high-risk group (**Figure 4B**).

To further elucidate the immunological relevance of the prognostic signature, correlations between the eight signature genes and immune cell infiltration were examined. The analysis demonstrated that the majority of immune cell subsets were significantly influenced by the expression levels of these genes (**Figure 4C**). In addition, differential expression analysis of immune checkpoint genes revealed higher expression levels in the high-risk group, including IDO2, TNFRSF8, TNFRSF25, CD244, CD27, TNFRSF14, NRP1, CD276, PDCD1, CD200R1, HAVCR2, CD80, CD28, TNFSF18, and TNFRSF8 (**Figure 4D**).

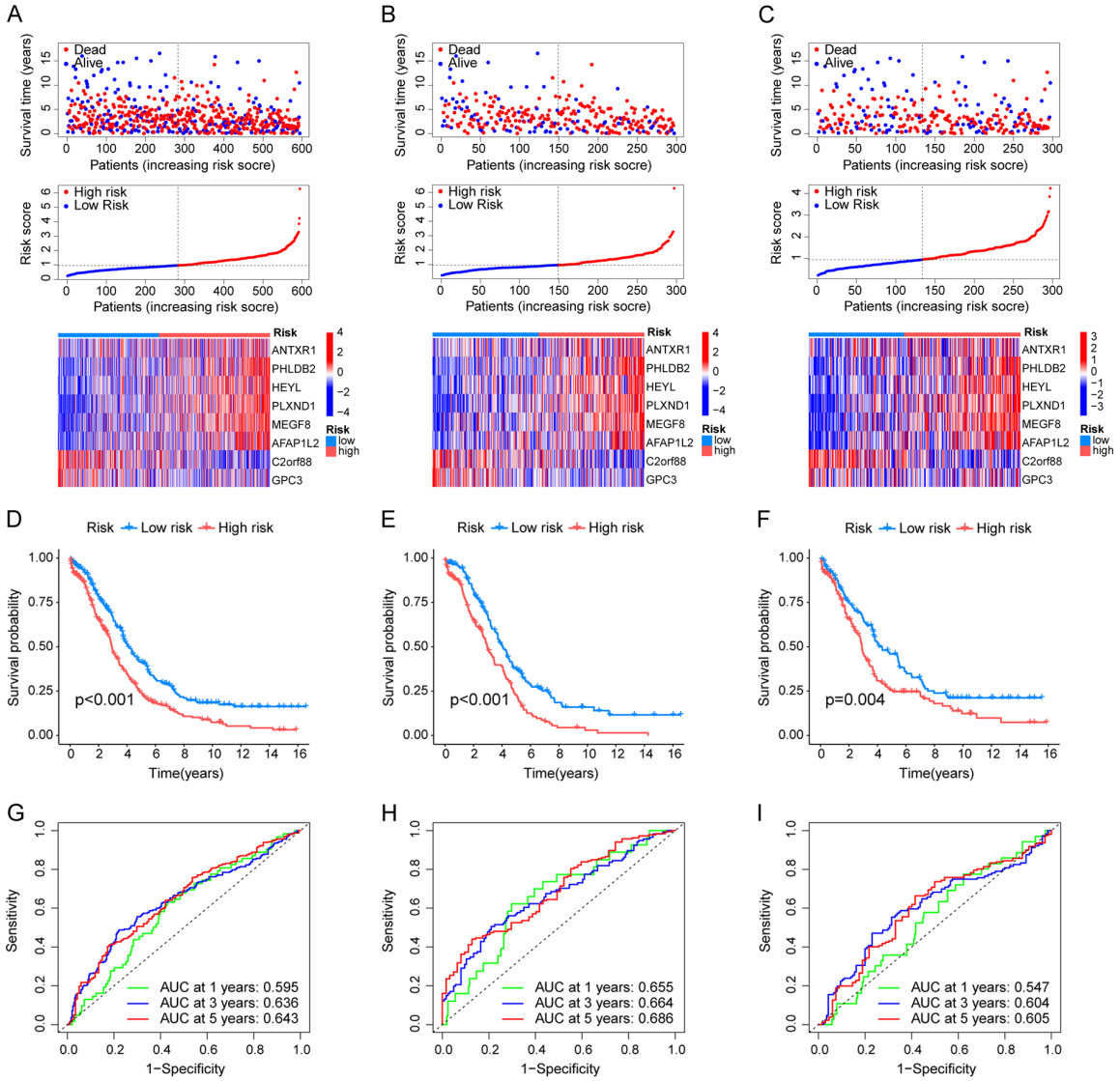

Figure 3. Prognostic risk model effectively stratifies patients in both training and test cohorts. A. The survival status and risk score distribution in the all patients. B. The survival status and risk score distribution in the train set. C. The survival status and risk score distribution in the test set. D. The Kaplan-Meier OS curves for patients in the high- and low-risk groups in the all patients. E. The Kaplan-Meier OS curves for patients in the high- and low-risk groups in the train set. F. The Kaplan-Meier OS curves for patients in the high- and low-risk groups in the test set. G-I. Receiver operating characteristic (ROC) curves showed the prognostic performance of the endometriosis-related prognostic risk model in all the patients, in the training set, and in the test set.

The TIDE algorithm was employed to estimate responses to immunotherapy based on transcriptomic profiles. Patients in the high-risk group exhibited significantly higher TIDE scores compared with those in the low-risk group, suggesting a greater likelihood of immune evasion (**Figure 4E**).

A drug sensitivity analysis was conducted to compare predicted therapeutic responses between the high- and low-risk groups, with higher estimated IC50 values indicating reduced drug sensitivity. Notably, ipatasertib, a selective AKT inhibitor, exhibited greater predicted efficacy in the low-risk group, suggesting enhanced susceptibility to AKT pathway inhibition in this subset (**Figure 4F**). Similarly, pictilisib, alpelisib, and buparlisib, targeting multiple isoforms of PI3K, showed significantly lower IC50 values in the low-risk group, indicating increased reliance on the PI3K/AKT signaling axis (**Figure 4G-I**). The selective PI3Kβ/δ inhibi-

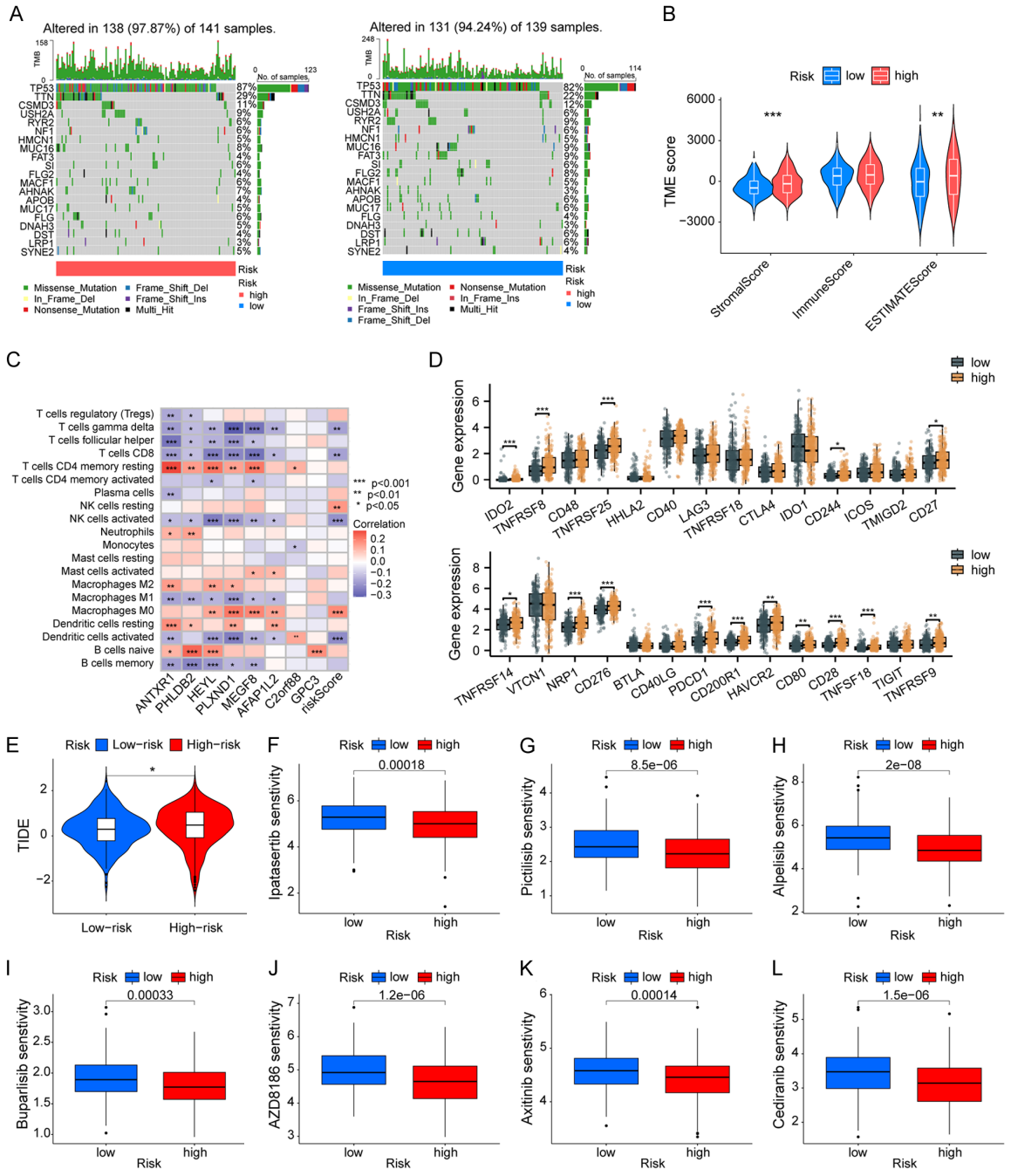

Figure 4. High-risk group exhibits an immunosuppressive microenvironment and may benefit from immunotherapy. A. The mutational landscape of patients in high- and low-risk groups. B. Tumor microenvironment (TME) score in high- and low-risk groups. C. Correlation between the immune cells, prognostic signature genes, and risk scores. D. The immune checkpoint gene expressions were different in the high-risk and low-risk groups. E. Comparison of tumor immune dysfunction and exclusion (TIDE) scores between high-risk group and low-risk group. F-L. Comparison of chemotherapy effect between high-risk group and low-risk group. *P < 0.05; **P < 0.01; ***P < 0.001.

tor AZD8186 further supported this vulnerability (**Figure 4J**). Moreover, axitinib and cediranib, both Vascular Endothelial Growth Factor Receptor (VEGFR) tyrosine kinase inhibitors, demonstrated enhanced predicted sensitivity in the low-risk group, implying a greater dependency on angiogenic pathways (**Figure 4K**, **4L**). Collectively, these findings underscore the potential clinical utility of PI3K/AKT/mTOR and VEGF signaling inhibitors as targeted treatment

strategies for patients characterized by low-risk molecular signatures.

Single-cell analysis reveals MEGF8 as a functional mediator of stem cell heterogeneity in OC

scRNA-seq data from 12 ovarian tissue samples - including 7 treatment-naïve high-grade serous ovarian cancer (HGSOC) samples encompassing both early- and late-stage tumors and 5 age-matched non-malignant ovarian samples - were integrated to systematically compare the expression profiles of eight prognostic signature genes across specific cellular subsets. Using the SingleR annotation tool, ten distinct cell subtypes were identified in both normal and tumor tissues, including natural killer cells, T cells, epithelial cells, monocytes, fibroblasts, B cells, endothelial cells, tissue stem cells, macrophages, and mesenchymal stem cells (**Figure 5A**). Overall expression scores of the signature genes were significantly higher in tumor samples compared with normal controls (**Figure 5B**). Subtype distribution analysis (**Figure 5C**) and Uniform Manifold Approximation and Projection (UMAP) visualization (**Figure 5D**) confirmed the accuracy of cell-type classification, supported by the differential expression patterns of canonical marker genes.

A focused analysis revealed heterogeneous expression patterns of the eight signature genes across the ten cell subtypes (**Figure 5E**). Notably, MEGF8 was highly expressed in multiple cell populations, including mesenchymal stem cells, macrophages, tissue stem cells, endothelial cells, and epithelial cells. Among these, epithelial cells in tumor tissues exhibited the highest MEGF8 expression, exceeding that of the other seven signature genes. Cross-sample comparisons further demonstrated consistently elevated MEGF8 expression in tumor-associated mesenchymal stem cells, tissue stem cells, endothelial cells, and epithelial cells, with the most pronounced differences observed in epithelial and tissue stem cells (**Figure 5F-H**).

Based on MEGF8 expression levels, tissue stem cells were stratified into high- and low-expression subgroups (**Figure 6A**). Quantitative analysis revealed a significantly higher proportion of MEGF8 high tissue stem cells in OC samples compared to normal tissues (**Figure 6B**). Gene Ontology (GO) enrichment analysis revealed that MEGF8 high cells were significantly enriched in biologic processes related to extracellular matrix structural constituents, electron transfer activity, and oxidoreductase-driven transmembrane transport (**Figure 6C**). KEGG pathway analysis further linked these cells to metabolism-associated pathways, including Parkinson's disease, prion disease, and oxidative phosphorylation (**Figure 6D**). A heatmap of Hallmark gene sets showed marked suppression of the Hedgehog signaling pathway in MEGF8 high cells, alongside significant activation of pro-survival pathways such as the unfolded protein response, reactive oxygen species (ROS) pathway, PI3K-AKT-mTOR signaling axis, and oxidative phosphorylation. In addition, lipid metabolism and DNA repair pathways were differentially regulated (**Figure 6E**). Taken together, these findings suggest that MEGF8 high tissue stem cells may contribute to functional heterogeneity during tumor progression by enhancing energy metabolism, remodeling the local microenvironment, and activating stress-adaptive signaling programs.

Pseudotime trajectory analysis suggested that MEGF8 high tissue stem cells were predominantly localized to earlier stages of differentiation (**Figure 6F-H**). Branch expression analysis modeling (BEAM) was applied to cluster dynamic gene expression changes along the pseudotime trajectory of tissue stem cell subpopulations (**Figure 6I**). The top 100 differentially expressed genes exhibited modular expression patterns across the differentiation continuum, revealing four distinct clusters (Clusters 1-4). Mitochondria-associated genes (e.g., MT-CO1, MT-ND1) and extracellular matrix genes (e.g., COL1A1, FN1) were enriched at early and late pseudotime stages, respectively, suggesting enhanced metabolic activity during early differentiation and matrix remodeling at later stages. In addition, spatially and temporally restricted expression of stress response genes (e.g., GADD45G, IER3) and immune regulatory genes (e.g., members of the HLA family) highlighted potential mechanisms by which MEGF8 high tissue stem cells maintain functional heterogeneity through metabolic reprogramming, microenvironmental interactions, and adaptive stress responses within the tumor microenvironment.

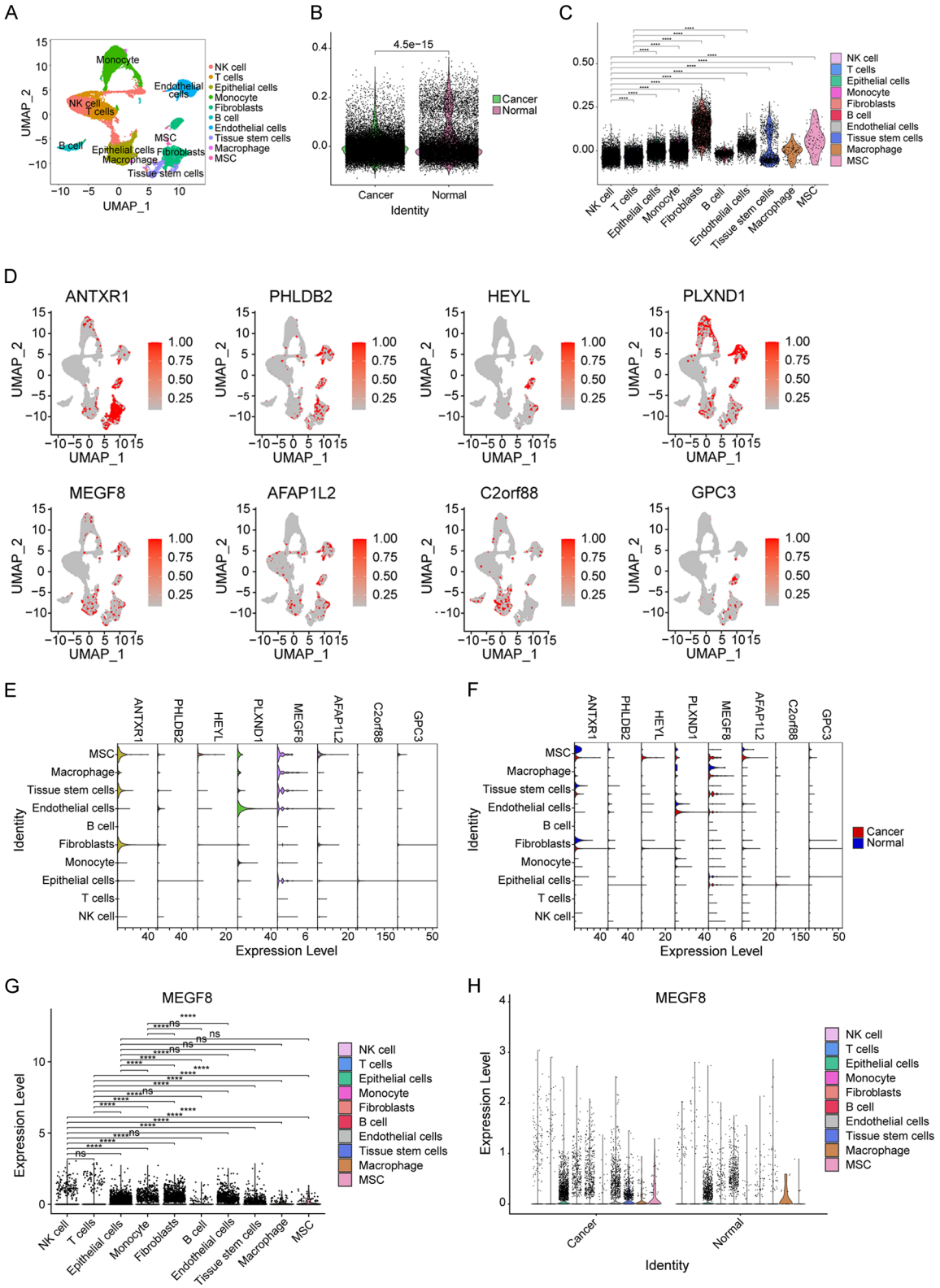

Figure 5. Single-cell transcriptomic atlas reveals cell-type-specific expression of signature genes. A. Uniform Manifold Approximation and Projection (UMAP) of the all samples. Colored by cell type. B. Levels of endometriosis-associated signature genes differ between normal and ovarian samples. C. The distribution of each cell subtype. D. Expression levels of signature genes for each cell subtype are plotted on the UMAP. The colour key from grey to red

indicated relative expression levels from low to high. E. Expression levels of 8 signature genes across 10 distinct cell subtypes. F. Expression levels of 8 signature genes in normal and ovarian samples. G. Expression levels of MEGF8 in ten distinct cell subtypes. H. Expression levels of MEGF8 in normal and ovarian samples. ****P < 0.0001; ns, P > 0.05.

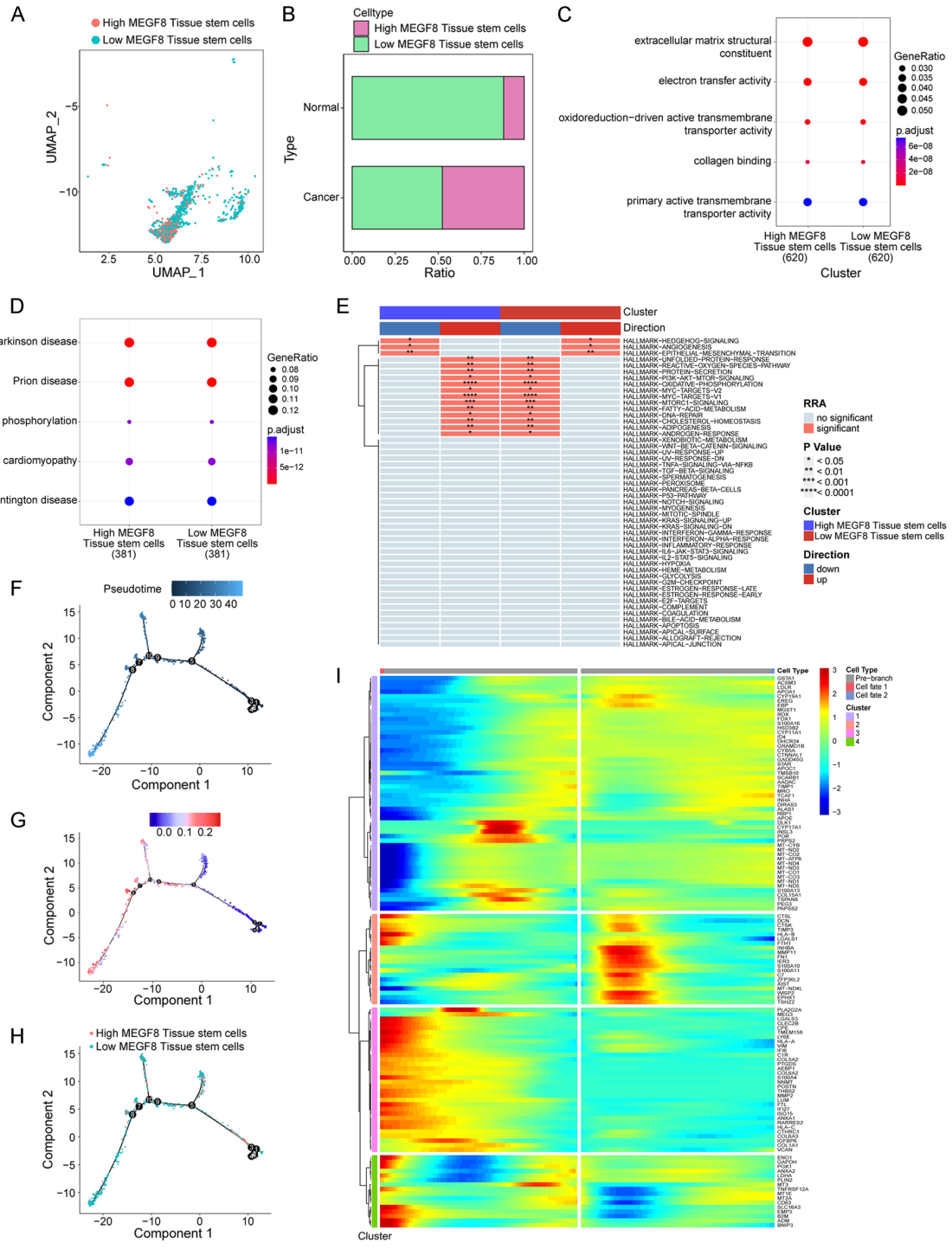

Figure 6. MEGF8-enriched tissue stem cells are associated with pro-tumorigenic pathways. A. UMAP plot of clustering high and low MEGF8 expression in stem cells. B. The proportion of high MEGF8 and low MEGF8 tissue stem cells in normal and ovarian samples. C, D. Bubble plot depicting the GO and KEGG enrichment analysis of high MEGF8 and low MEGF8 tissue stem cells, elucidating their associated biological functions and diseases. E. Heatmap showing different pathways enriched in high MEGF8 and low MEGF8 tissue stem cells by GSVA. F-H. Pseudo-time analysis of tissue stem cells. I. Pseudo-time heatmap showing the expression dynamics of key genes.

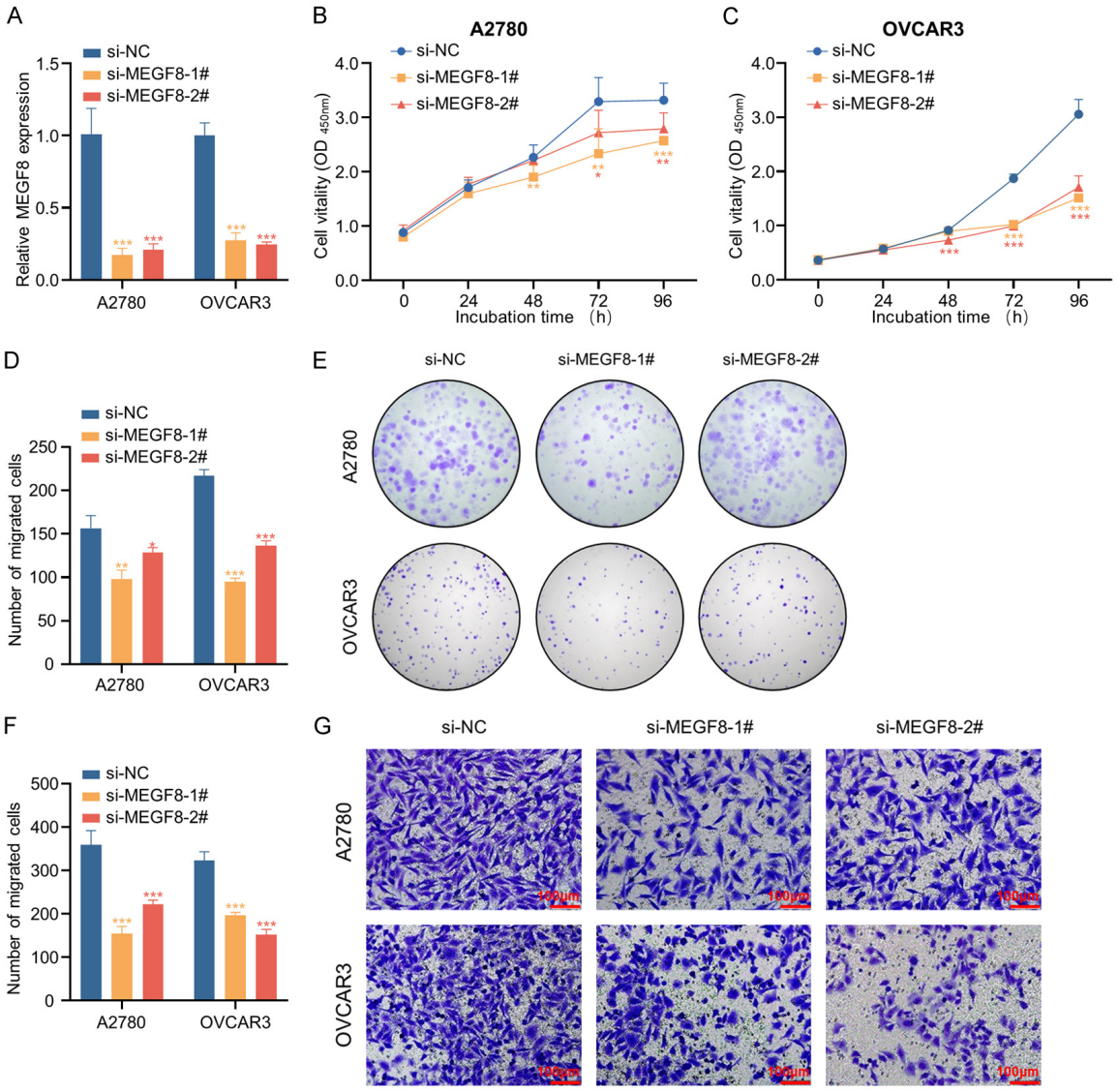

Figure 7. MEGF8 knockdown inhibits ovarian cancer cell proliferation and migration. A. Relative expression levels of MEGF8 were measured by quantitative real-time polymerase chain reaction (qRT-PCR) in A2780 and OVCAR3 cells transfected with si-NC, si-MEGF8-#1, or si-MEGF8-#2 (n = 3 for each group). The internal control was 18S rRNA. B, C. Cell Counting Kit-8 (CCK8) assays detected the OC cells viability with MEGF8 silencing, n = 6. D, E. The proliferation ability of cells transfected with si-MEGF8 was assessed by colony formation assays, n = 3. F, G. The migration ability of cells transfected with si-MEGF8 was examined by transwell assays, n = 3 (×200). Scale bar: 100 μm. *P < 0.05, **P < 0.01, ***P < 0.001.

MEGF8 knockdown inhibits the proliferation and migration and promotes the apoptosis of A2780 and OVCAR3 cells

To further investigate the functional role of MEGF8 in OC cells, in vitro experiments were performed using A2780 and OVCAR3 cell lines. MEGF8 expression was silenced by siRNA (siMEGF8), and quantitative PCR confirmed a significant reduction in MEGF8 mRNA levels in the siMEGF8 group compared with the negative control (siNC) group (**Figure 7A**). Cell proliferation was assessed using CCK-8 and colony formation assays, both of which demonstrated that MEGF8 knockdown led to a marked decrease in the proliferative capacity of A2780 and OVCAR3 cells (**Figure 7B-E**). Furthermore, Transwell migration assays revealed that MEGF8 silencing significantly impaired the migratory ability of both cell lines (**Figure 7F** and **7G**).

Discussion

The development, chemoresistance, and unfavorable prognosis of OC have been promoted by endometriosis through the remodeling of the TME and its synergy with genetic mutations [28]. The construction of a precision predictive model based on immune characteristics and chemosensitivity, alongside the in-depth elucidation of key molecular mechanisms, is expected to provide strong support for optimizing individualized immunotherapy and chemotherapy strategies, thereby improving patient prognosis [29]. Through integrative multi-omics analysis, three molecular subtypes associated with ERGs, designated as endometriosis-associated groups A-C, were identified. Among them, group B was found to be associated with better survival outcomes ($P = 0.001$). This classification was closely linked to differential activation of multiple pathways within the TME. Group A tumors were characterized by features related to invasion and metastasis, such as epithelial-mesenchymal transition and activation of the TGF-β signaling pathway, and were enriched in pathways commonly observed in small cell lung cancer and prostate cancer, suggesting a more aggressive phenotype with potential metastatic propensity. The favorable prognosis observed in group B was likely attributable to increased infiltration of activated $CD8^+$ T cells and NK cells in the immune microenvironment, both of which serve as critical effector cells in antitumor immunity and are capable of directly eliminating tumor cells [30, 31]. Concurrently, a reduction in immunosuppressive cell populations (e.g., Treg, Th2) in group B may have attenuated the immunosuppressive effects within the TME, thereby enhancing antitumor immune responses [32]. This molecular classification offers a novel tool for individualized prognostic assessment in OC. For instance, patients with group A tumors may require more intensive treatment strategies, such as targeted therapies against invasion-associated pathways, whereas patients with group B tumors may benefit from immunotherapeutic approaches.

Through LASSO regression and multivariate Cox analysis, eight feature genes (GPC3, C2orf88, AFAP1L2, MEGF8, PLXND1, HEYL, PHLDB2, and ANTXR1) were identified as being significantly associated with OS, and a risk model with clinical prognostic value was subsequently constructed. These genes were found to play multidimensional regulatory roles in tumor progression. GPC3 (Glypican-3), a member of the heparan sulfate proteoglycan family, has been reported to be highly expressed in several solid tumors, including hepatocellular carcinoma and ovarian clear cell carcinoma, and may promote tumor proliferation and metastasis through the Wnt/β-catenin and Hedgehog pathways [33]. Although previous studies have emphasized its role as a recurrence biomarker, GPC3 was found to be significantly upregulated in the high-risk group in the present study, suggesting that it may contribute to malignant progression in endometriosis-associated OC through distinct microenvironmental interactions. ANTXR1 (TEM8), a collagen receptor, has been proposed to mediate the immunosuppressive effects of chemotherapy-resistant myofibroblasts through regulation of the YAP1 signaling pathway [34]; its high expression was consistent with poor prognosis observed in patients. AFAP1L2 and MEGF8 were highly expressed in the low-risk group, and genomic instability analysis revealed a higher frequency of copy number deletions for both genes, indicating their potential roles as "genomic guardians" that may suppress tumor progression [35]. HEYL, a downstream transcription factor of the Notch signaling pathway, has been previously implicated in promoting epithelial-mesenchymal transition (EMT) and tumor metastasis [36]. However, in the present model, high HEYL expression was associated with the low-risk group. This apparent contradiction may reflect a cell type-specific function of HEYL in OC or suggest possible crosstalk with other pathways such as PI3K/AKT, warranting further mechanistic investigation.

The immune biological basis underlying risk stratification was elucidated through TME analysis. A pronounced immunosuppressive profile was observed in the high-risk group. An elevated TIDE score suggested that immune evasion in high-risk tumors may be mediated by the recruitment of regulatory T cells and upregulation of immune checkpoint molecules such as PDCD1, CD276, and NRP1. Enrichment of stromal scores and metabolic pathways, including cytochrome P450, in the high-risk group indicated that tumor cells might adapt to microenvironmental stress via a "metabolism-ECM

remodeling" axis, thereby promoting chemoresistance. This finding was consistent with single-cell data demonstrating a stem cell - like oxidative phosphorylation dependence of MEGF8. Although limited responsiveness to immune checkpoint inhibitors was predicted in the high-risk group, increased sensitivity (reflected by lower IC_{50} values) to PI3K/AKT/mTOR pathway inhibitors (e.g., ipatasertib, pictilisib) and antiangiogenic agents (e.g., axitinib) was observed. This may be attributable to compensatory activation of the PI3K/AKT pathway and a heightened reliance on VEGFR-mediated angiogenesis in high-risk tumors. In contrast, enhanced immune infiltration - such as increased $CD8^+$ T cells - was identified in the low-risk group, potentially making these tumors more amenable to immune-targeted combination therapies. The risk model constructed in this study demonstrated moderate predictive performance in both training and validation cohorts (AUC for 1-year and 5-year OS: 0.655-0.686), a range commonly reported in comparable studies [37, 38]. Its translational potential lies in two key aspects. First, integrating molecular subtypes (e.g., endometriosis-associated subtype B) with risk scoring enables refined prognostic stratification; for instance, high-risk subtype A patients may require intensified surveillance and multi-target interventions. Second, TME-informed drug sensitivity profiling suggests that high-risk patients may benefit from PI3K/AKT inhibition combined with antiangiogenic therapy, whereas low-risk patients may derive greater benefit from immune checkpoint blockade.

scRNA-seq analysis further revealed the cell type - specific expression and functional networks of key genes in OC. MEGF8 was found to be highly expressed across a wide range of cell types, including mesenchymal stem cells, macrophages, tissue stem cells, endothelial cells, and epithelial cells, underscoring its multifaceted regulatory roles in the pathophysiology of OC. Given that ovarian epithelial cells are the cells of origin for epithelial OC - which accounts for approximately 90% of all OC cases - their abnormal proliferation or mutation has been implicated in malignant transformation [39]. In this study, MEGF8 was specifically overexpressed in tumor epithelial cells, and its expression level was positively correlated with tissue stemness scores (**Figure 5F-H**), suggesting a role in tumorigenesis through maintenance of epithelial stemness. This hypothesis was validated through functional experiments, where MEGF8 silencing significantly inhibited proliferation and migration, while inducing apoptosis in epithelial OC cell lines (A2780, OVCAR3) (**Figure 7A-G**). Pseudotime trajectory analysis demonstrated that tissue stem cells with high MEGF8 expression were enriched at early differentiation stages (**Figure 6F-H**), and this was accompanied by the activation of mitochondrial respiratory chain genes (e.g., MT-CO1) and stress response genes (e.g., GADD45G). In conjunction with KEGG enrichment results - highlighting pathways such as oxidative phosphorylation and ECM-receptor interaction - it is proposed that MEGF8 may promote stem cell plasticity via a "metabolism-ECM remodeling" axis: on one hand, enhancing oxidative phosphorylation to meet the high energy demand; on the other, remodeling the stem cell niche by regulating ECM components such as COL1A1 and FN1, thereby sustaining self-renewal capacity (**Figure 6I**). These findings provide a multi-scale line of evidence supporting the oncogenic role of MEGF8: at the single-cell level, its expression is linked to stem cell differentiation status; at the molecular level, it modulates metabolic and microenvironmental signaling pathways; and at the cellular level, it directly affects malignant phenotypes.

Moreover, since MEGF8 is a transmembrane protein containing multiple EGF-like domains, it is likely to interact with receptors involved in cell adhesion and migration, key processes in cancer metastasis. Although the exact receptor through which MEGF8 exerts its effects in OC have not yet been characterized, the precise molecular mechanisms by which MEGF8 regulates oxidative phosphorylation and ECM remodeling are critical to understanding its functional roles in OC. Identifying the receptor responsible for MEGF8 activity in both tumor cells and the TME is essential for future targeted therapeutic strategies. As a secreted protein, blocking MEGF8 with monoclonal antibodies or adding additional MEGF8 may alter tumor cell behavior by either inhibiting or enhancing these receptor interactions, potentially affecting tumor growth, migration, and immune cell infiltration in the TME. Further studies should explore these therapeutic possibilities to better understand the implications of MEGF8 in OC and its potential as a therapeutic target.

Despite revealing the molecular heterogeneity of OC through integrative multi-omics analysis, this study has several limitations. First, generalizability may be limited by the retrospective nature of the datasets used (TCGA and GEO), which are subject to selection bias and lack standardized documentation of treatment variables (e.g., surgical extent, chemotherapy-regimens), thus constraining analysis of treatment-induced immune remodeling. Future prospective, multi-center studies incorporating standardized clinical and pathological parameters are warranted to enhance the model's clinical applicability. Second, mechanistic insights remain incomplete. While functional assays confirmed the oncogenic role of MEGF8, the precise molecular mechanisms by which it regulates oxidative phosphorylation and ECM remodeling - such as involvement of receptor tyrosine kinases or non-coding RNAs-remain to be elucidated. CRISPR-based functional screens or spatial transcriptomics may enable systematic exploration of the MEGF8 interaction network at the tumor-stroma interface.

Conclusion

Through integrative multi-omics analysis and functional validation, this study elucidated the molecular heterogeneity of endometriosis-associated OC and identified a core mechanism by which MEGF8 drives tumor progression via a "metabolism-ECM remodeling" axis. Single-cell analyses revealed that MEGF8 is specifically overexpressed in tumor stem-like cells and sustains stemness by activating oxidative phosphorylation and ECM reorganization. Functional experiments confirmed that MEGF8 silencing significantly suppressed cellular proliferation and migration while inducing apoptosis. A risk model based on MEGF8-related signatures suggested that high-risk patients exhibit an immunosuppressive tumor microenvironment - characterized by Treg cell infiltration and upregulation of immune checkpoints (e.g., PD-1, CD276) - as well as a dependency on the PI3K/AKT signaling pathway, conferring increased sensitivity to targeted therapies. In contrast, the low-risk group, with active immune infiltration, may benefit from immune-based combination strategies. Collectively, these findings establish MEGF8 as a potential diagnostic biomarker and therapeutic target, offering novel mechanistic insights and translational directions for overcoming chemoresistance and improving prognosis in OC.

Acknowledgements

This work was supported by the Suzhou Gu Su Health Talent Research Project (GSWS2023-011), Suzhou Science and Education to Promote Health Youth Science and Technology Project (KJXW2022030), and Suzhou Applied Basic Research (Medical and Health) Youth Project (SYW2025137).

Disclosure of conflict of interest

None.

Address correspondence to: Guannan Feng, Department of Gynaecology, The Affiliated Suzhou Hospital of Nanjing Medical University, Suzhou Municipal Hospital, Gusu School, Nanjing Medical University, Suzhou 215002, Jiangsu, China. Tel: +86-17715882298; E-mail: fengguannan@njmu.edu.cn; Chao Huang and Qingxia Meng, State Key Laboratory of Reproductive Medicine and Offspring Health, Center for Reproduction and Genetics, The Affiliated Suzhou Hospital of Nanjing Medical University, Suzhou Municipal Hospital, Gusu School, Nanjing Medical University, Suzhou 215002, Jiangsu, China. Tel: +86-18652886677; E-mail: zjhc2007@126.com (CH); Tel: +86-18068005518; E-mail: mqx593204@163.com (QXM); Xiaoyan Huang, State Key Laboratory of Reproductive Medicine and Offspring Health, Department of Histology and Embryology, School of Basic Medical Sciences, Nanjing Medical University, Nanjing 211166, Jiangsu, China. Tel: +86-13915946650; E-mail: bbhxy@njmu.edu.cn

References

[1] Lheureux S, Braunstein M and Oza AM. Epithelial ovarian cancer: evolution of management in the era of precision medicine. CA Cancer J Clin 2019; 69: 280-304.

[2] Cho KR and Shih Ie M. Ovarian cancer. Annu Rev Pathol 2009; 4: 287-313.

[3] Webb PM and Jordan SJ. Epidemiology of epithelial ovarian cancer. Best Pract Res Clin Obstet Gynaecol 2017; 41: 3-14.

[4] Stewart C, Ralyea C and Lockwood S. Ovarian cancer: an integrated review. Semin Oncol Nurs 2019; 35: 151-156.

[5] Kuroki L and Guntupalli SR. Treatment of epithelial ovarian cancer. BMJ 2020; 371: m3773.

[6] Pujade-Lauraine E and Combe P. Recurrent ovarian cancer. Ann Oncol 2016; 27 Suppl 1: i63-i65.
[7] Pearce CL, Templeman C, Rossing MA, Lee A, Near AM, Webb PM, Nagle CM, Doherty JA, Cushing-Haugen KL, Wicklund KG, Chang-Claude J, Hein R, Lurie G, Wilkens LR, Carney ME, Goodman MT, Moysich K, Kjaer SK, Hogdall E, Jensen A, Goode EL, Fridley BL, Larson MC, Schildkraut JM, Palmieri RT, Cramer DW, Terry KL, Vitonis AF, Titus LJ, Ziogas A, Brewster W, Anton-Culver H, Gentry-Maharaj A, Ramus SJ, Anderson AR, Brueggmann D, Fasching PA, Gayther SA, Huntsman DG, Menon U, Ness RB, Pike MC, Risch H, Wu AH and Berchuck A; Ovarian Cancer Association Consortium. Association between endometriosis and risk of histological subtypes of ovarian cancer: a pooled analysis of case-control studies. Lancet Oncol 2012; 13: 385-394.
[8] Tung KH, Goodman MT, Wu AH, McDuffie K, Wilkens LR, Kolonel LN, Nomura AM, Terada KY, Carney ME and Sobin LH. Reproductive factors and epithelial ovarian cancer risk by histologic type: a multiethnic case-control study. Am J Epidemiol 2003; 158: 629-638.
[9] Giudice LC and Kao LC. Endometriosis. Lancet 2004; 364: 1789-1799.
[10] As-Sanie S, Black R, Giudice LC, Gray Valbrun T, Gupta J, Jones B, Laufer MR, Milspaw AT, Missmer SA, Norman A, Taylor RN, Wallace K, Williams Z, Yong PJ and Nebel RA. Assessing research gaps and unmet needs in endometriosis. Am J Obstet Gynecol 2019; 221: 86-94.
[11] Saunders PTK and Horne AW. Endometriosis: etiology, pathobiology, and therapeutic prospects. Cell 2021; 184: 2807-2824.
[12] Wang Y, Nicholes K and Shih IM. The origin and pathogenesis of endometriosis. Annu Rev Pathol 2020; 15: 71-95.
[13] Kordowitzki P, Mechsner S and Sehouli J. ARID1a gene as a potential early marker to tackle endometriosis-associated ovarian cancer. Aging Dis 2023; 15: 2331-2333.
[14] Sato T, Saito M, Nakajima S, Saito K, Katagata M, Fukai S, Okayama H, Sakamoto W, Saze Z, Momma T, Mimura K and Kono K. ARID1A deficiency is targetable by AKT inhibitors in HER2-negative gastric cancer. Gastric Cancer 2023; 26: 379-392.
[15] Khan S, Budamagunta V and Zhou D. Targeting KRAS in pancreatic cancer: emerging therapeutic strategies. Adv Cancer Res 2023; 159: 145-184.
[16] Linder A, Westbom-Fremer S, Mateoiu C, Olsson Widjaja A, Österlund T, Veerla S, Ståhlberg A, Ulfenborg B, Hedenfalk I and Sundfeldt K. Genomic alterations in ovarian endometriosis and subsequently diagnosed ovarian carcinoma. Hum Reprod 2024; 39: 1141-1154.
[17] Westerberg AC, Degnes ML, Andresen IJ, Roland MCP and Michelsen TM. Angiogenic and vasoactive proteins in the maternal-fetal interface in healthy pregnancies and preeclampsia. Am J Obstet Gynecol 2024; 231: 550.e1-550.e22.
[18] Wilkerson MD and Hayes DN. ConsensusClusterPlus: a class discovery tool with confidence assessments and item tracking. Bioinformatics 2010; 26: 1572-1573.
[19] Hänzelmann S, Castelo R and Guinney J. GSVA: gene set variation analysis for microarray and RNA-seq data. BMC Bioinformatics 2013; 14: 7.
[20] Yoshihara K, Shahmoradgoli M, Martínez E, Vegesna R, Kim H, Torres-Garcia W, Treviño V, Shen H, Laird PW, Levine DA, Carter SL, Getz G, Stemke-Hale K, Mills GB and Verhaak RG. Inferring tumour purity and stromal and immune cell admixture from expression data. Nat Commun 2013; 4: 2612.
[21] Newman AM, Liu CL, Green MR, Gentles AJ, Feng W, Xu Y, Hoang CD, Diehn M and Alizadeh AA. Robust enumeration of cell subsets from tissue expression profiles. Nat Methods 2015; 12: 453-457.
[22] Satija R, Farrell JA, Gennert D, Schier AF and Regev A. Spatial reconstruction of single-cell gene expression data. Nat Biotechnol 2015; 33: 495-502.
[23] Hu S and Wang M. Identification of a deubiquitinating gene-related signature in ovarian cancer using integrated transcriptomic analysis and machine learning framework. Discov Oncol 2025; 16: 510.
[24] Zhang P, Feng J, Rui M, Xie J, Zhang L and Zhang Z. Integrating machine learning and single-cell analysis to uncover lung adenocarcinoma progression and prognostic biomarkers. J Cell Mol Med 2024; 28: e18516.
[25] Hu H, Xi X, Jiang B, Wang K, Wu T, Chen X, Guo Y, Zhou T, Huang X, Yu J, Gao T, Wu Y and Zheng B. RNF187 facilitates proliferation and migration of human spermatogonial stem cells through WDR77 polyubiquitination. Cell Prolif 2025; 58: e70042.
[26] Wu T, Zhou H, Wang L, Tan J, Gao W, Wu Y, Zhao D, Shen C, Zheng B, Huang X and Shao B. TRIM59 is required for mouse GC-1 cell maintenance through modulating the ubiquitination of AXIN1. Heliyon 2024; 10: e36744.
[27] Xu BY, Yu XL, Gao WX, Gao TT, Hu HY, Wu TT, Shen C, Huang XY, Zheng B and Wu YB. RNF187 governs the maintenance of mouse GC-2 cell development by facilitating histone H3 ubiquitination at K57/80. Asian J Androl 2024; 26: 272-281.

[28] Henlon Y, Panir K, McIntyre I, Hogg C, Dhami P, Cuff AO, Senior A, Moolchandani-Adwani N, Courtois ET, Horne AW, Rosser M, Ott S and Greaves E. Single-cell analysis identifies distinct macrophage phenotypes associated with prodisease and proresolving functions in the endometriotic niche. Proc Natl Acad Sci U S A 2024; 121: e2405474121.

[29] Lu Z and Gao Y. Screening differentially expressed genes between endometriosis and ovarian cancer to find new biomarkers for endometriosis. Ann Med 2021; 53: 1377-1389.

[30] Yang YL, Yang F, Huang ZQ, Li YY, Shi HY, Sun Q, Ma Y, Wang Y, Zhang Y, Yang S, Zhao GR and Xu FH. T cells, NK cells, and tumor-associated macrophages in cancer immunotherapy and the current state of the art of drug delivery systems. Front Immunol 2023; 14: 1199173.

[31] Domagala J, Grzywa TM, Baranowska I, Justyniarska M, Tannir R, Graczyk-Jarzynka A, Kusowska A, Lecka M, Poreba M, Fidyt K, Marhelava K, Pilch Z, Picard LK, Wegierski T, Jastrzebski K, Krawczyk M, Klopotowska M, Granica M, Urlaub D, Hajduk S, Neeser A, Moros S, Kozlowski P, Bobrowicz M, Miaczynska M, Ma L, Watzl C and Winiarska M. Ammonia suppresses the antitumor activity of natural killer cells and t cells by decreasing mature perforin. Cancer Res 2025; 85: 2448-2467.

[32] Si F, Liu X, Tao Y, Zhang Y, Ma F, Hsueh EC, Puram SV and Peng G. Blocking senescence and tolerogenic function of dendritic cells induced by γδ Treg cells enhances tumor-specific immunity for cancer immunotherapy. J Immunother Cancer 2024; 12: e008219.

[33] Shimizu Y, Suzuki T, Yoshikawa T, Endo I and Nakatsura T. Next-generation cancer immunotherapy targeting glypican-3. Front Oncol 2019; 9: 248.

[34] Licaj M, Mhaidly R, Kieffer Y, Croizer H, Bonneau C, Meng A, Djerroudi L, Mujangi-Ebeka K, Hocine HR, Bourachot B, Magagna I, Leclere R, Guyonnet L, Bohec M, Guérin C, Baulande S, Kamal M, Le Tourneau C, Lecuru F, Becette V, Rouzier R, Vincent-Salomon A, Gentric G and Mechta-Grigoriou F. Residual ANTXR1+ myofibroblasts after chemotherapy inhibit anti-tumor immunity via YAP1 signaling pathway. Nat Commun 2024; 15: 1312.

[35] Kang EY, Weir A, Meagher NS, Farrington K, Nelson GS, Ghatage P, Lee CH, Riggan MJ, Bolithon A, Popovic G, Leung B, Tang K, Lambie N, Millstein J, Alsop J, Anglesio MS, Ataseven B, Barlow E, Beckmann MW, Berger J, Bisinotto C, Bösmüller H, Boros J, Brand AH, Brooks-Wilson A, Brucker SY, Carney ME, Casablanca Y, Cazorla-Jiménez A, Cohen PA, Conrads TP, Cook LS, Coulson P, Courtney-Brooks M, Cramer DW, Crowe P, Cunningham JM, Cybulski C, Darcy KM, El-Bahrawy MA, Elishaev E, Erber R, Farrell R, Fereday S, Fischer A, García MJ, Gayther SA, Gentry-Maharaj A and Gilks CB; AOCS Group; Grube M, Harnett PR, Harrington SP, Harter P, Hartmann A, Hecht JL, Heikaus S, Hein A, Heitz F, Hendley J, Hernandez BY, Polo SH, Heublein S, Hirasawa A, Høgdall E, Høgdall CK, Horlings HM, Huntsman DG, Huzarski T, Jewell A, Jimenez-Linan M, Jones ME, Kaufmann SH, Kennedy CJ, Khabele D, Kommoss FKF, Kruitwagen RFPM, Lambrechts D, Le ND, Lener M, Lester J, Leung Y, Linder A, Loverix L, Lubiński J, Madan R, Maxwell GL, Modugno F, Neuhausen SL, Olawaiye A, Olbrecht S, Orsulic S, Palacios J, Pearce CL, Pike MC, Quinn CM, Mohan GR, Rodríguez-Antona C, Ruebner M, Ryan A, Salfinger SG, Sasamoto N, Schildkraut JM, Schoemaker MJ, Shah M, Sharma R, Shvetsov YB, Singh N, Sonke GS, Steele L, Stewart CJR, Sundfeldt K, Swerdlow AJ, Talhouk A, Tan A, Taylor SE, Terry KL, Tołoczko A, Traficante N, Van de Vijver KK, van der Aa MA, Van Gorp T, Van Nieuwenhuysen E, van-Wagensveld L, Vergote I, Vierkant RA, Wang C, Wilkens LR, Winham SJ, Wu AH, Benitez J, Berchuck A, Candido Dos Reis FJ, DeFazio A, Fasching PA, Goode EL, Goodman MT, Gronwald J, Karlan BY, Kommoss S, Menon U, Sinn HP, Staebler A, Brenton JD, Bowtell DD, Pharoah PDP, Ramus SJ and Köbel M. CCNE1 and survival of patients with tubo-ovarian high-grade serous carcinoma: an ovarian tumor tissue analysis consortium study. Cancer 2023; 129: 697-713.

[36] Katoh M and Katoh M. Integrative genomic analyses on HES/HEY family: notch-independent HES1, HES3 transcription in undifferentiated ES cells, and Notch-dependent HES1, HES5, HEY1, HEY2, HEYL transcription in fetal tissues, adult tissues, or cancer. Int J Oncol 2007; 31: 461-466.

[37] Zhao Z, Sun C, Hou J, Yu P, Wei Y, Bai R and Yang P. Identification of STEAP3-based molecular subtype and risk model in ovarian cancer. J Ovarian Res 2023; 16: 126.

[38] Luo X, Wang Y, Zhang H, Chen G, Sheng J, Tian X, Xue R and Wang Y. Identification of a prognostic signature for ovarian cancer based on ubiquitin-related genes suggesting a potential role for FBXO9. Biomolecules 2023; 13: 1724.

[39] Torre LA, Trabert B, DeSantis CE, Miller KD, Samimi G, Runowicz CD, Gaudet MM, Jemal A and Siegel RL. Ovarian cancer statistics, 2018. CA Cancer J Clin 2018; 68: 284-296.